Research Square

Preprints are preliminary reports that have not undergone peer review.
They should not be considered conclusive, used to inform clinical practice,
or referenced by the media as validated information.

Visualizing 5d-Mediated Electronic Interactions in Pt–Ln Complexes via Resonant Inelastic X-ray Scattering

Takefumi Yoshida

tyoshyd@wakayama-u.ac.jp

Wakayama University https://orcid.org/0000-0003-3479-7890

Yujiro Ochi
Keiichi Katoh
Ryo Masuda
Shinji Kitao
Takuma Kaneko
Tomoya Uruga
Yasuhiro Iwasawa
Masahiro Yamashita

Article

Keywords:

Posted Date: June 22nd, 2026

DOI: https://doi.org/10.21203/rs.3.rs-9950532/v1

License: This work is licensed under a Creative Commons Attribution 4.0 International License.
Read Full License

Additional Declarations: There is **NO** Competing Interest.

Abstract

Heterometallic complexes exhibit unique electronic structures arising from intermetallic interactions, which are difficult to visualize experimentally. This work investigates multinuclear Ln–Pt complexes (Ln = Tb (**1**) and Dy (**2**)) using Ln L_3-edge resonant inelastic X-ray scattering (RIXS) coupled with Quanty-based atomic multiplet calculations. The resulting Ln L_3-edge 2p3d RIXS spectra exhibit modified d–f multiplet features along with an additional shoulder in the intermediate energy-loss region. Compared with conventional mononuclear lanthanide complexes, these Pt–Ln architectures display unusually well-resolved multiplet-derived features, indicating a substantial perturbation of the Ln-centered electronic states by the heterometallic coordination environment. Atomic multiplet simulations incorporating the crystal-field splitting of Ln 5d orbitals successfully replicate the overall spectral trends and greater multiplet complexity observed in the Dy system. These results demonstrate that Ln L_3-edge RIXS is a sensitive probe for detecting hidden heterometallic electronic interactions in multinuclear lanthanide complexes.

Introduction

Heterometallic complexes, including discrete molecules[1,2], metal–organic frameworks (MOFs)[3], supramolecular cages[4,5], and coordination polymers[6], have attracted considerable interest because of their potential applications in catalysis[3,5], electronic devices[6,7], luminescence[8], and magnetism[9-13]. Heterometallic interactions can generate electronic structures and functionalities unattainable in monometallic systems[1,2,14]. For example, heterometallic Al-based MOFs containing M^{2+}/Al^{3+} trimeric clusters (M = Mg, Mn, Co, or Ni) exhibit tunable porosities and highly selective gas adsorption[3]. In addition, metal–ligand and metal–metal interactions in heterometallic Mo_2M' chains respond asymmetrically to electron-donating ligands, revealing an unexpected redistribution of electronic effects along the metal chain[15]. These studies highlight the importance of clarifying intermetallic electronic interactions to understand and control the physical properties of heterometallic systems.

Resonant inelastic X-ray scattering (RIXS) is an element-specific photon-in photon-out spectroscopic technique capable of probing the electronic states of target elements with high sensitivity[16,17]. For example, the systematic analysis of M_4-edge multiplet features in U, Np, Pu, and Am compounds enables the direct comparison of 5f-electron localization and bonding characteristics across the actinide series[18]. Furthermore, intra-atomic d–f electron interactions in trivalent lanthanides have been studied using 2p3d RIXS measurements[19]. In addition, lanthanide (Ln) L-edge RIXS and high-energy-resolution fluorescence detected X-ray absorption near edge structure can sensitively probe ligand-field effects and metal–ligand covalency in f-element coordination compounds[20]. Specifically, La L_2-edge core-to-core RIXS directly reflects metal–ligand covalency via modifications of the La-centered 4f and 5d electronic structures[20]. These studies have established Ln L-edge RIXS as a powerful tool for investigating local electronic and bonding interactions in f-element chemistry.

Moreover, Pt L_3-edge RIXS has been shown to reflect interactions between Pt 5d states and the surrounding coordination environments with high sensitivity[14]. Recent studies on Pt-containing multinuclear complexes have revealed characteristic inelastic scattering features associated with axial electronic interactions that were not observed in square-planar reference compounds[21]. Density-of-states analyses suggested that these additional excitations originated from electronic coupling between the Pt d and Ln d states mediated through axial coordination channels. These observations indicate that RIXS can be used to detect hidden heterometallic electronic interactions that cannot be resolved by conventional X-ray absorption spectroscopy.

Despite these advances, experimental investigations of heterometallic interactions from the perspective of lanthanide electronic states remain limited, and most studies have focused on theoretical calculations. In particular, the influence of heterometallic coupling on Ln-centered intra-atomic d–f interactions in Ln L_3-edge RIXS spectra is yet to be elucidated.

To address these gaps in the literature, this study investigates two multinuclear Ln–Pt heterometallic complexes, NEt_4{[Pt(PhSAc)$_4$]Ln[(PhSAc)$_4$Pt]}·2DMF (Ln = Tb (**1**), Dy (**2**); PhSAc = thiobenzoate; DMF = *N,N*-dimethylformamide), using hard X-ray RIXS combined with Quanty-based multiplet and hybridization calculations. By probing both the Pt- and Ln-centered electronic states, we show that RIXS enables the visualization of hidden heterometallic electronic interactions associated with the perturbation of Ln 5d orbitals. Pt L_3-edge RIXS revealed characteristic intermediate-energy excitations associated with axial Pt–Ln electronic coupling, whereas Ln L_3-edge 2p3d RIXS revealed modified d–f multiplet structures that deviated from the purely atomic model. The combined experimental and theoretical results demonstrate that heterometallic Pt–Ln coordination significantly perturbs Ln-centered electronic structures in a manner detectable by Ln L_3-edge RIXS. More broadly, this study bridges the gap between the structural characterization and electronic-state analysis of heterometallic complexes, providing new insights into how Pt–Ln coordination influences Ln electronic structures beyond conventional ligand-field models.

Results and Discussion

Structural Basis for Pt–Ln Electronic Interactions

The multinuclear Ln–Pt complexes Tb (**1**) and Dy (**2**) adopt isostructural paddlewheel-like architectures composed of two Pt centers bridged by a central lanthanide ion (**Fig. 1**). The crystallographic details are listed in **Table S1**. The Tb ion is coordinated to eight oxygen atoms and two Pt ions to form a bicapped square-antiprismatic geometry, whereas each Pt center adopts a square-pyramidal coordination environment consisting of four sulfur atoms and one axial Tb ion. The intramolecular Tb–Pt distances are 3.608(1) and 3.623(1) Å for the Tb complex. Although these distances are approximately 10% shorter than the sum of the van der Waals radii of Tb and Pt (4.02 Å), they exceed the reported covalent (~3.30 Å) and ionic (~3.10 Å) radii. Such extended Ln–Pt separations make direct heterometallic interactions difficult to identify using conventional structural analysis alone. However, the axial arrangement of the Ln

ion relative to the Pt center is expected to influence the Pt d_z^2-derived electronic states and associated heterometallic electronic coupling.

Pt L_3-edge RIXS Reveals Hidden Heterometallic Interactions

To probe hidden heterometallic electronic interactions, Pt and Ln L_3-edge RIXS measurements were performed on complexes **1** and **2**[21]. Compared with the mononuclear square-planar Pt complex $(NBt_4)_2$ $[Pt(dmit)_2]$, the multinuclear Ln–Pt complexes exhibit an additional inelastic scattering feature at approximately 6 eV in the energy-loss direction, whereas both systems show characteristic Pt 5d-derived (~4 eV) and ligand-related (~8 eV) excitations[21]. To clarify the origin of this 6 eV feature, Quanty-based multiplet and hybridization calculations were performed using four- and six-coordinate electronic structure models. The four-coordinate model, which incorporates only in-plane hybridization associated with square-planar Pt–S interactions, replicated the ~4 and ~8 eV excitations but failed to generate the 6 eV feature (**Fig. S1a**). In contrast, the inclusion of axial hybridization channels selectively coupled to the Pt d_z^2 orbital produced an additional 6 eV excitation while preserving the other spectral features (**Fig. S1b**). Density-of-state analyses further supported the hypothesis that this excitation originated from axial electronic coupling between the Ln d states and Pt d orbitals within the heterometallic coordination environment. Overall, these results demonstrated that Pt L_3-edge RIXS can be used to directly visualize hidden heterometallic electronic interactions that are not observed in conventional XANES measurements.

Ln L_3-edge RIXS Reveals Modified d–f Multiplet Structures

Compared to conventional mononuclear Ln complexes, these heterometallic Pt–Ln complexes exhibit unusually well-resolved multiplet-derived structures in their Ln L_3-edge RIXS spectra. This observation suggests that the Pt–Ln coordination environment induces a substantially stronger perturbation of the Ln 5d electronic states than typical organic ligand fields, enabling the direct spectroscopic visualization of heterometallic effects at the lanthanide site.

The overall Tb L_3-edge 2D RIXS map for complex **1** is broadly consistent with previously reported Ln 2p3d RIXS spectra dominated by intra-atomic d–f multiplet interactions (**Fig. 2a**)[19]. In particular, the inelastic scattering features in the 10–14 eV region correspond well to the characteristic multiplet excitations reported for trivalent lanthanide systems. In contrast to conventional atomic-like Ln RIXS spectra, complex **1** exhibits unusually well-resolved and partially separated multiplet-derived inelastic scattering features, suggesting that the heterometallic Pt–Ln coordination environment significantly perturbs the Tb-centered electronic structure.

To further analyze these Tb-centered electronic excitations, the transfer-energy profiles extracted from the 2D RIXS maps of **1** were deconvoluted into multiple inelastic scattering components (**Fig. 2b**). The spectrum was reproduced using partially overlapping components centered at approximately 7.3, 10.1,

12.8, and 15.5 eV. Although Tb^{3+} systems generally exhibit lower multiplet complexity than Dy^{3+} systems, the Pt–Tb complex requires several partially resolved inelastic components to reproduce the experimental spectral envelope. This behavior suggests partial separation of the multiplet-derived inelastic structures

arising from the heterometallic Pt–Ln coordination environment.

In addition to the dominant multiplet-derived structures, an inelastic scattering feature is observed at approximately 7 eV that cannot be explained within conventional purely atomic-like multiplet descriptions reported for mononuclear lanthanide systems. Notably, this energy region closely corresponds to the additional excitation previously identified via Pt L_3-edge RIXS measurements of multinuclear Pt–Ln complexes. Furthermore, this additional Ln-centered component is located approximately 2–3 eV away from the dominant multiplet-derived structures, which is an energy separation comparable to that observed for the Pt-centered intermediate-energy excitation. These similarities suggest that a common heterometallic electronic interaction associated with the axial Pt–Ln coordination environment contributes to both the Pt- and Ln-centered RIXS responses.

Compared with the Tb L_3-edge 2D RIXS map of the conventional $TbPc_2$ double-decker complex $[Tb(Pc)_2]TBA$ (**Fig. S2a**), which exhibits a relatively smooth and predominantly fluorescence-like spectral envelope, the multinuclear complex **1** displays more clearly resolved and partially separated inelastic structures along the energy transfer axis. In conventional mononuclear lanthanide complexes containing only organic ligand fields, the perturbation of the spatially extended Ln 5d states is generally weak, leading to broad, partially overlapping multiplet envelopes. In contrast, the anisotropic Pt–Ln coordination environment in the present multinuclear complex introduces additional axial perturbations to the Ln 5d orbitals, resulting in enhanced splitting and separation of multiplet-derived inelastic scattering features.

The overall Dy L_3-edge 2D RIXS map for complex **2** is broadly consistent with the previously reported Ln 2p3d RIXS spectra dominated by intra-atomic d–f multiplet interactions[19]. However, compared with the Tb system, the Dy L_3-edge RIXS map exhibits more clearly separated energy-loss features with pronounced splitting-like spectral characteristics along the energy-transfer axis, consistent with the stronger multiplet complexity expected for the Dy^{3+} electronic configuration. In particular, the dominant inelastic scattering features observed in the 10–16 eV region match the characteristic multiplet excitations reported for conventional trivalent lanthanide systems[19].

To further analyze the Dy-centered electronic excitations, the transfer-energy profiles extracted from the 2D RIXS maps of complex **2** were deconvoluted into multiple inelastic scattering components (**Fig. 2d**). The experimental spectrum was fitted using partially overlapping components centered at approximately 7.3, 10.4, 13.2, 15.8, and 18.8 eV. The spectra could not be replicated using a single broad fluorescence-like feature, indicating the presence of multiple resolved electronic excitations and a substantially

stronger multiplet complexity than that of the Tb system. In particular, the Dy system exhibited a broader distribution of multiplet-derived inelastic structures extending to higher energy-transfer regions.

In addition to the dominant multiplet-derived structures, an inelastic feature is observed at approximately 7 eV, suggesting an additional contribution beyond conventional atomic multiplet descriptions that neglect perturbation of the Ln 5d orbitals. Similar to the Tb system, this Dy-centered component is observed approximately 2–3 eV away from the dominant multiplet-derived structures, an energy separation comparable to that observed for the Pt-centered intermediate energy feature. The additional high-energy components observed only in the Dy system likely reflect the greater intrinsic multiplet complexity associated with the Dy^{3+} $4f^9$ electronic configuration.

Compared to the conventional atomic-like Ln RIXS spectra and the relatively smooth fluorescence-like spectral envelope observed for TBA[$Dy(Pc)_2$] (**Fig. S2b**), the spectrum of multinuclear complex **2** exhibits better resolved and partially separated inelastic scattering features. The more pronounced splitting observed for the Dy system further indicates that heterometallic perturbation is strongly coupled to the intrinsic multiplet complexity of the Ln electronic configuration.

Additional DC magnetic susceptibility and spectroscopic measurements indicate predominantly paramagnetic behavior with no clear evidence of strong magnetic exchange coupling, suggesting that the observed Pt–Ln interactions primarily modify the local electronic structure rather than generate strong bulk magnetic interactions (**Fig. S3**).

The combined Pt and Ln L_3-edge RIXS results further suggest that the heterometallic interaction is not limited to the Pt 5d–Ln 5d electronic coupling. Ln L_3-edge 2p3d RIXS process directly involving the Ln 5d intermediate and final states, and the crystal-field splitting of the Ln 5d orbitals strongly influences the observed multiplet-derived inelastic structures. Because the Ln L_3-edge 2p3d RIXS spectra are strongly governed by intra-atomic d–f multiplet interactions, the modification and splitting of the Ln-centered inelastic scattering features imply an indirect coupling between the Pt-centered electronic states and the Ln 4f manifold mediated through crystal-field-perturbed Ln 5d orbitals. The heterometallic origin of these spectral changes is strongly supported by the common intermediate-energy scale observed in both the Pt- and Ln-centered RIXS spectra, as well as the absence of comparable features in conventional mononuclear lanthanide reference systems. Furthermore, the substantially enhanced separation and redistribution of the multiplet-derived inelastic structures observed in the present Pt–Ln systems suggest that the heterometallic coordination environment induces a significantly greater perturbation of the Ln 5d electronic states than typical organic ligand-field environments alone. These results indicate that Pt–Ln heterometallic coordination can substantially modify Ln-centered multiplet structures in a manner detectable by Ln L_3-edge RIXS.

Quanty-Based RIXS Simulations of Ln L_3-edge RIXS

To further investigate the origin of the observed spectral features, Quanty-based atomic multiplet calculations were performed for the Tb and Dy L_3-edge 2p3d RIXS processes[22-24]. These calculations incorporated 4f–4f, 2p–4f, 3d–4f, and 4f–5d Coulomb interactions; spin–orbit coupling of the core, 4f, and 5d states; and crystal-field splitting of the Ln 5d orbitals (details are provided in Supplementary Information S3). Crystal-field splitting of the Ln 5d orbitals was introduced to effectively represent the anisotropic perturbation imposed by the heterometallic Pt–Ln coordination environment. Consequently, the crystal-field parameters should not be interpreted as quantitatively determined ligand-field energies.

In contrast to Pt L_3-edge calculations, which incorporated explicit axial hybridization channels and successfully reproduced intermediate-energy features, the corresponding Ln calculations employed a simplified atomic multiplet model that omitted explicit heterometallic hybridization. Directly including Pt–Ln hybridization channels in Ln L_3-edge 2p3d RIXS calculations substantially expands the multiplet configuration space and increases the computational cost. Therefore, this study utilizes a reduced model that accounts for the Ln 5d crystal-field splitting and intra-atomic 4f–5d interactions to capture the dominant qualitative spectral features.

In the calculations, the transfer energy scale corresponds to the calculated final-state energy differences. Because the simplified Ln multiplet model does not explicitly account for the elastic scattering channel, the calculated spectra were compared with the experimental data, primarily in terms of relative spectral evolution and the sequence of inelastic features, rather than absolute energy separation from the elastic line. Consequently, although a shoulder-like spectral contribution was reproduced in the calculated spectra, the absolute transfer-energy positions of the experimental features were not quantitatively reproduced.

Nevertheless, the calculations successfully reproduce several key experimental spectral characteristics. For the Tb system, the calculated spectrum exhibits a shoulder-like onset around ~22 eV followed by a broad multiplet-derived envelope extending above ~24 eV. Experimentally, the Tb RIXS spectrum contains an intermediate-energy component (~7.3 eV) together with higher-energy multiplet-derived structures (~10.1, 12.8, and 15.5 eV). Although the simplified atomic multiplet model does not quantitatively reproduce the absolute transfer-energy positions of the experimental features, the overall spectral morphology is qualitatively similar. For the Dy system, the calculated spectrum exhibits a broader and more structured distribution of multiplet-derived spectral weight extending from approximately 14 eV to higher transfer energies. The calculation reproduces the progressive separation and increased complexity of the inelastic structures observed experimentally. In particular, the calculated Dy spectrum displays a more structured multiplet envelope than the Tb calculation, consistent with the experimentally resolved components centered at approximately 7.3, 10.4, 13.2, 15.8, and 18.8 eV. The enhanced separation of the multiplet-derived structures in the Dy calculation is consistent with the experimentally observed increase in spectral complexity in the Dy L_3-edge RIXS spectra.

These results support the assignment of the dominant high-energy-loss structures to intra-atomic d–f multiplet excitations that are further modified by perturbation of the Ln 5d crystal-field environment arising from the heterometallic Pt–Ln coordination structure. In addition, a weak shoulder-like intensity is consistently observed at approximately 6–7 eV in both calculated and experimental spectra. The deconvoluted experimental RIXS spectra indicate that this intermediate-energy component is better described as a partially overlapping shoulder-like inelastic feature, rather than a discrete excitation peak. The calculated results for Dy also show stronger splitting and greater separation of the inelastic multiplet structures than those for Tb, which is consistent with the observed enhancement of the spectral complexity in the experimental Dy L_3-edge RIXS spectra. These results suggest that the Ln-centered multiplet features indirectly reflect perturbation of the Ln 4f manifold mediated through Pt-induced modification of the Ln 5d crystal-field environment.

The results of Pt L_3-edge Quanty calculations further demonstrate that the intermediate-energy feature is significantly enhanced upon the inclusion of the axial Pt d_{z^2}-related coupling. Combined with the Ln L_3-edge RIXS results, these observations suggest that heterometallic interactions manifest differently at the Pt and Ln sites. Explicit axial hybridization dominates the Pt-centered response, whereas crystal-field perturbations of the Ln 5d orbitals and intra-atomic d–f multiplet interactions primarily govern the Ln-centered multiplet features. Thus, the combined experimental and theoretical results demonstrate that RIXS can sensitively visualize hidden heterometallic electronic interactions that extend beyond purely atomic descriptions.

Conclusion

This study demonstrates that Ln L_3-edge RIXS is a sensitive probe for heterometallic perturbations in Ln coordination compounds. Compared with conventional mononuclear systems, the unusually well-resolved multiplet structures in these Pt–Ln complexes indicate that heterometallic coordination can significantly modify the Ln-centered electronic states by perturbing the Ln 5d orbitals. These findings establish Ln L_3-edge RIXS as a powerful approach for visualizing subtle electronic interactions that cannot be detected using conventional structural, magnetic, or absorption techniques. More broadly, combining element-selective RIXS with multiplet-based electronic structure modeling establishes a general framework for investigating hidden electronic interactions in heterometallic molecular systems. This approach is likely applicable to a wide range of lanthanide- and actinide-containing materials, providing new opportunities for understanding and designing functional molecular systems with tunable magnetic, luminescent, and electronic properties.

Methods

Synthesis and Structural Characterization

The detailed synthesis procedures for **1** and **2** are outlined in Supplementary Information S1. Single-crystal X-ray diffraction measurements were performed using a Rigaku XtaLAB Synergy DW system.

Ln L3-edge RIXS Measurements

For sample preparation, the powdered materials were used as synthesized and pressed into self-supported pellets (10 mm diameter) using a hydraulic press without the addition of binders or diluents. Subsequently, Ln L_3-edge RIXS measurements were performed at the BL36XU beamline of SPring-8. The beamline spectrometer uses eight sets of spherically bent Si (620) and Ge (444) analyzer crystals configured for the Tb L_3-edge and Dy L_3-edge, respectively. A 2D X-ray pixel array detector (Merlin Quad, Quantum Detectors) was used to detect the X-rays diffracted by the analyzer crystals[17]. The experimental spectra were normalized to their maximum inelastic scattering intensity after subtracting the elastic scattering contribution, where appropriate. The transfer-energy profiles extracted from the 2D RIXS maps were fitted using multiple Gaussian components. To avoid over-parameterization, the peak widths were fixed at a common full width at half maximum (2.5 eV) during the deconvolution analysis. These fits were then used to estimate the approximate energy positions of the partially overlapping inelastic components, rather than providing a unique quantitative decomposition of the spectral envelope.

Quanty-Based Multiplet and Hybridization Calculations

Pt L_3-edge RIXS spectra were analyzed using Quanty-based multiplet and hybridization calculations[22-24]. Four- and six-coordinate electronic structural models were constructed to simulate the square-planar and axially coordinated Pt environments, respectively. The four-coordinate model includes only in-plane Pt–S hybridization channels, whereas the six-coordinate model also incorporates axial hybridization channels selectively coupled to the Pt d_z^2 orbital. Coulomb interactions, spin–orbit coupling, crystal-field splitting, and hybridization effects were included in the Hamiltonians.

The Ln L_3-edge 2p3d RIXS spectra were analyzed using Quanty-based atomic multiplet calculations. The calculations included 4f–4f, 2p–4f, 3d–4f, and 4f–5d Coulomb interactions; spin–orbit coupling of the core, 4f, and 5d states; and crystal-field splitting of the Ln 5d orbitals. The intermediate states are described as $2p^5 3d^{10} 4f^n 5d^1$ configurations, and the final states are $2p^6 3d^9 4f^n 5d^1$ configurations. Certain atomic multiplet parameters and scaling procedures were adapted from previous Quanty-based Ln L3-edge 2p3d RIXS studies[12]. No charge-transfer bath or explicit Pt–Ln hybridization channels were introduced in the Ln calculations. Lorentzian broadening parameters were applied to account for core-hole lifetime and instrumental resolution effects. The complete calculation parameters are provided in Supplementary Information S3.

Data Availability

The data supporting this study are presented in this article and in the Supplementary Information. The X-ray crystallographic data for the structures reported in this work were deposited at the Cambridge Crystallographic Data Centre (CCDC) under the deposition numbers CCDC 2559472 and 2559476. These data can be obtained free of charge from the CCDC at www.ccdc.cam.ac.uk/data_request/cif.

Declarations

Acknowledgements

This research was supported by JSPS KAKENHI (grant numbers JP20K15293 (T.Y.), 23K13761 (T. Y.), and 26K01516 (T. Y.) from the Yamada Science Foundation. The HERFD-XANES and RIXS measurements were performed using the BL36XU beamline at SPring-8. Part of this study was supported by the New Energy and Industrial Technology Development Organization (NEDO). We would like to thank Editage (www.editage.jp) for English language editing.

Author contributions

Y.O. contributed to the synthesis and solution of the crystal structure; K. K. contributed to the synthesis and RIXS measurements; R. M. and S. K. contributed to Mössbauer measurements; T. K. and T. U. contributed to the RIXS measurements; Y. I. and M. Y. reviewed and edited the manuscript; T. Y. contributed to the synthesis and RIXS measurements, wrote the original draft, and managed the research.

Competing interests

The authors declare no competing financial interests.

References

1. Zhou, N. *et al*. Effective near-infrared triplet emitter based on hetero-metal–metal interaction. *J. Am. Chem. Soc.***147**, 19949–19958 (2025).
2. Macaluso, E. *et al*. A heterometallic [LnLn'Ln] lanthanide complex as a qubit with embedded quantum error correction. *Chem. Sci.* **11**, 10337– 10343 (2020).
3. Wang, W., Chen, Y., Bu, X., Feng, P. Heterometallic aluminum metal–organic frameworks. *J. Am. Chem. Soc.***147**, 15146–15156 (2025).
4. Thoonen, S. *et al*. Single-step synthesis of a heterometallic $[Cu_2PdL_4]^{2+}$ hybrid metal–organic coordination cage. *Angew. Chem. Int. Ed.* **64**, e202506064 (2025).
5. Moree, L. K., Faulkner, L. A. V., Crowley, J. D. Heterometallic cages: synthesis and applications. *Chem. Soc. Rev.***53**, 25-46 (2024).
6. Bera, M. K., Sarmah, S., Santra, D. C., Higuchi, M. Heterometallic supramolecular polymers: From synthesis to properties and applications. *Coord. Chem. Rev.***501**, 215573 (2024).
7. Yu, W. *et al*. Novel composite separators based on heterometallic metal–organic frameworks improve the performance of lithium-ion batteries. *Adv. Energy Mater.***13**, 2204055 (2023).
8. Ye, J. *et al* Giant 3d-4f heterometallic polyoxoniobates of $\{Na_2Zn_{29}Ln_{12}Nb_{122}\}$, $\{Zn_{10}Eu_8Nb_{60}\}$, and $\{Zn_{16}Ln_8Nb_{88}\}$ with photonic barcodes. *Small***21**, e06482 (2025).

9. Larsen, E. M. H., Vosch, T., Bendix, J. Ductile metallophilic interactions and their mediation of magnetic interactions in [Ni{Pt(SAc)$_4$}(pyNO$_2$)]$_2$ complexes. *Inorg. Chem.***64**, 5366–5374 (2025).
10. Pantelis, K. N., Raptopoulou, C. P., Psycharis, V., Tang, J., Stamatatos, T.C. Square planar Pd(ii)/oximate complexes as 'metalloligands' for the directional assembly of 4f-metal ions: a new family of {Ln$_2$Pd} (Ln = lanthanide) clusters exhibiting slow magnetization relaxation. *Dalton Trans*. **54**, 977-988 (2025).
11. Costa-Villén, E., Puigjaner, C., Mayans, J., Escuer, A. Dodecanuclear Mn^{II}–Gd^{III} metallomacrocycles: magnetic and refrigerant responses. *Dalton Trans.***55**, 1298-1305 (2026).
12. Feltham , H. L. C., Brooker , S. Review of purely 4f and mixed-metal Nd-4f single-molecule magnets containing only one lanthanide ion. *Coord. Chem. Rev.***276**, 1-33 (2014).
13. Yoshida, T. *et al*. Insight into the Gd–Pt bond: Slow magnetic relaxation of a heterometallic Gd–Pt complex. *Bull. Chem. Soc. Jpn*. **95**, 513–521 (2022).
14. Yoshida, T. *et al*. Ionic-caged heterometallic bismuth–platinum complex exhibiting electrocatalytic CO_2 reduction. *Dalton Trans.***49**, 2652–2660 (2020).
15. Walde, R.K., Pankratz, T.C., Wheaton, A.M., Acosta, M., Berry, J.F. *Chem. Eur. J.***31**, 202090 (2025).
16. Jarrige, I. *et al*. Toward optimizing the performance of self-regenerating Pt-based perovskite catalysts. *ACS Catal*. **5**, 1112–1118 (2015).
17. Uruga, T. *et al*. SPring-8 BL36XU: synchrotron radiation X-ray-based multi-analytical beamline for polymer electrolyte fuel cells under operating conditions. *Chem. Rec.***19**, 1444–1456 (2019).
18. Schacherl, B. *et al*. Resonant inelastic X-ray scattering tools to count 5 f electrons of actinides and probe bond covalency. *Nat. Commun.***16**, 1221 (2025).
19. Zasimov, P., Amidani, L., Retegan, M., Walter, O., Caciuffo, R., Kvashnina, K. O. HERFD-XANES and RIXS study on the electronic structure of trivalent lanthanides across a series of isostructural compounds. *Inorg. Chem.***61**, 1817–1830 (2022).
20. Ramanantoanina, H. *et al*. High-energy resolution X-ray spectroscopy reveals bonding characteristics of La3+ homologues of actinium radiopharmaceuticals. *Commun. Chem.***9**, 148 (2026).
21. Yoshida, T. *et al.* Hidden heterometallic interaction emerging from resonant inelastic X-ray scattering in luminescent Tb–Pt molecules. *J. Phys. Chem. C***126**, 7973–7979 (2022).
22. Hoeppner, Y. L. M., Gunnarsson, O. & Haverkort, M. W. Efficient real-frequency solver for dynamical mean-field theory. *Phys. Rev. B***90**, 085102 (2014).
23. Haverkort, M. W. *et al*. Bands, resonances, edge singularities and excitons in core level spectroscopy investigated within the dynamical mean-field theory. *Euro. Phys. Lett.* **108**, 57004 (2014).
24. Haverkort, M. W., Zwierzcki, M, & Andersen, O. K., Multiplet ligand-field theory using Wannier orbitals. *Phys. Rev. B***85**, 165113 (2012).

Figures

Figure 1.

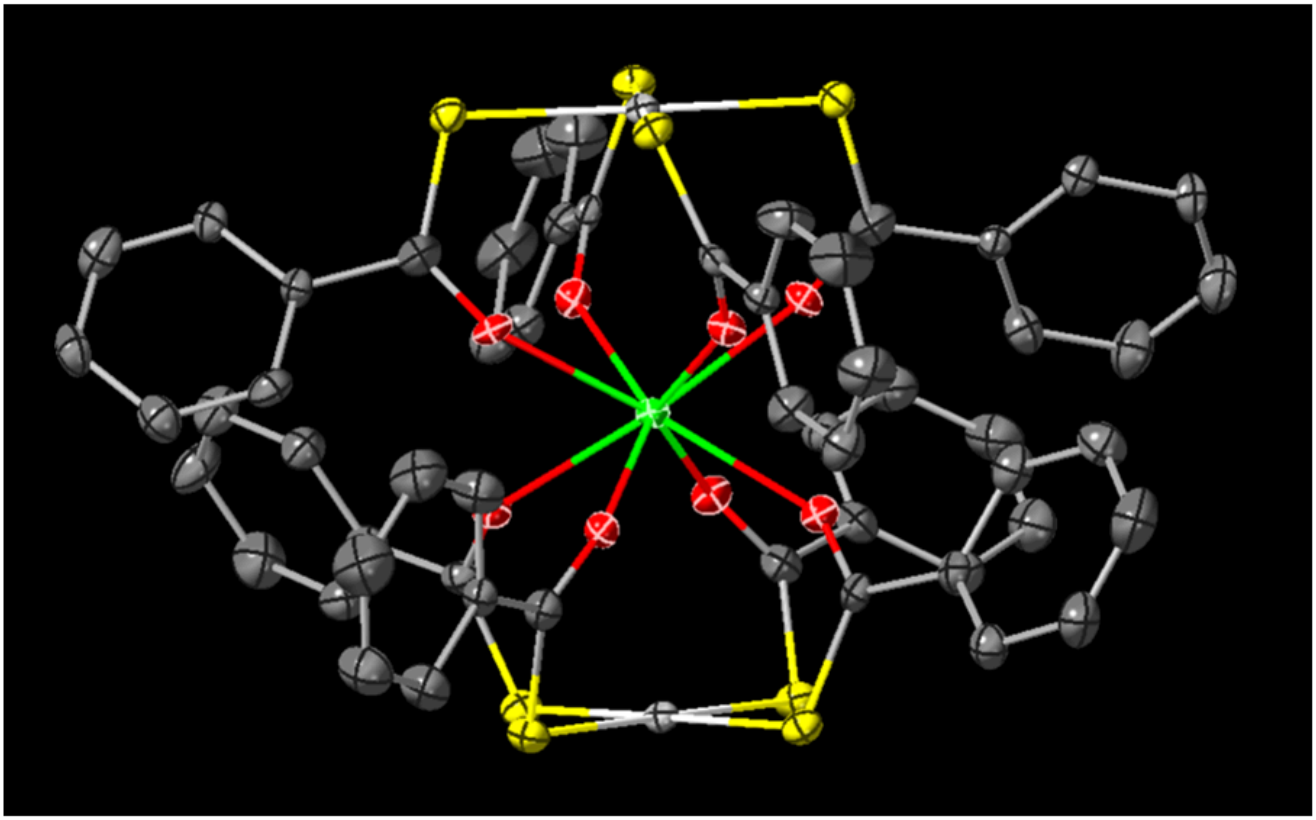


Figure 1

Crystal structure of complexes **1** and **2**. Tb or Dy, Pt, S, O, and C atoms are shown in green, silver, yellow, red, and gray, respectively. Thermal ellipsoids are drawn at the 40% probability level. Hydrogen atoms, DMF molecules, and tetraethylammonium counter cations are omitted for clarity.

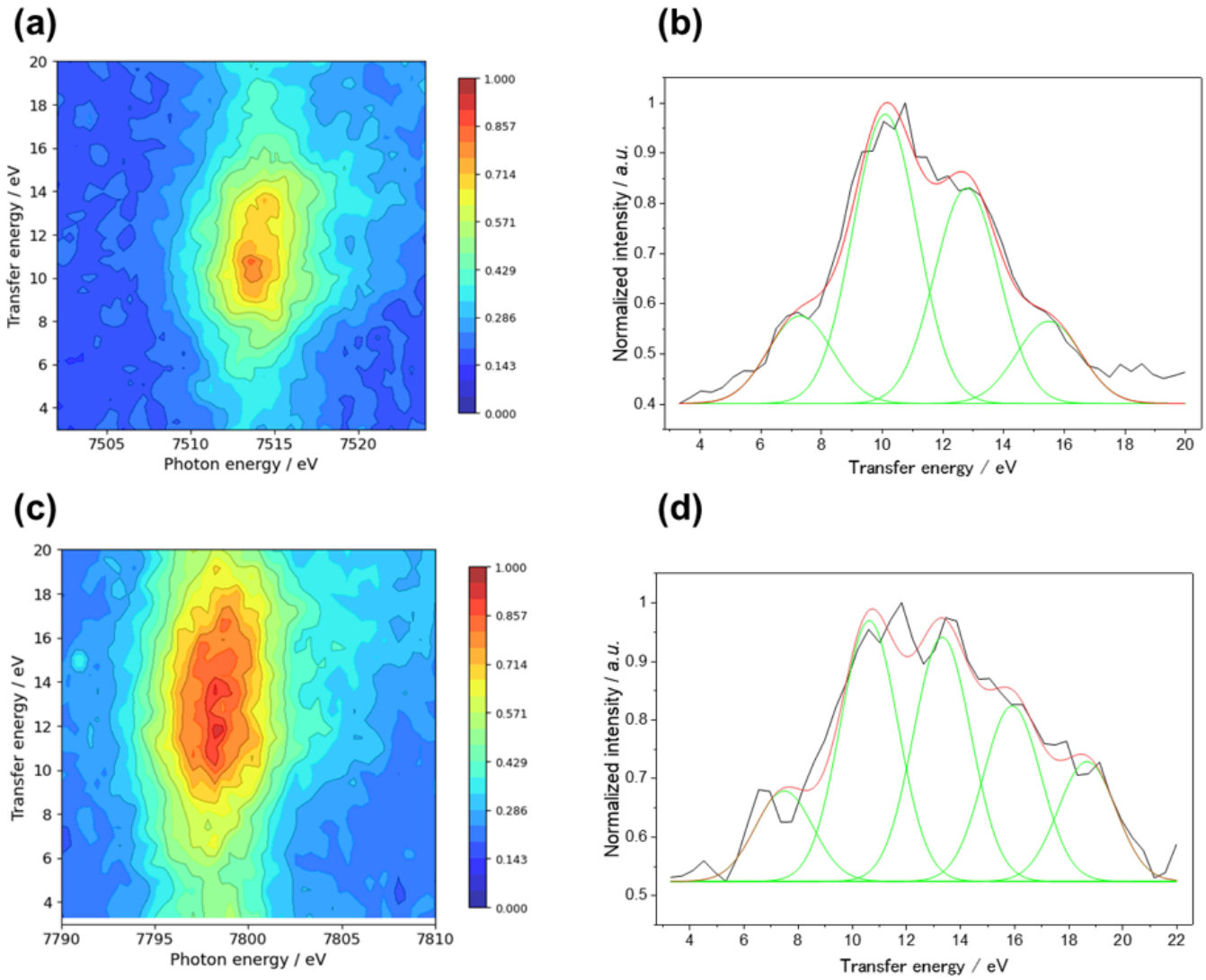


Figure 2

(a, c) Experimental Ln L_3-edge 2D RIXS maps and (b, d) corresponding transfer-energy profiles of (a, b) complex **1** (Tb) and (c, d) complex **2** (Dy). In panels (b) and (d), the black lines represent the experimental spectra, the red lines indicate the overall fitting results, and the green lines denote the individual Gaussian components. To avoid overparameterization, all Gaussian components were fit using a common full width at half maximum of 2.5 eV. This deconvolution analysis was used to estimate the approximate energy positions of partially overlapping inelastic components rather than to provide a unique, quantitative decomposition of the spectral envelope.

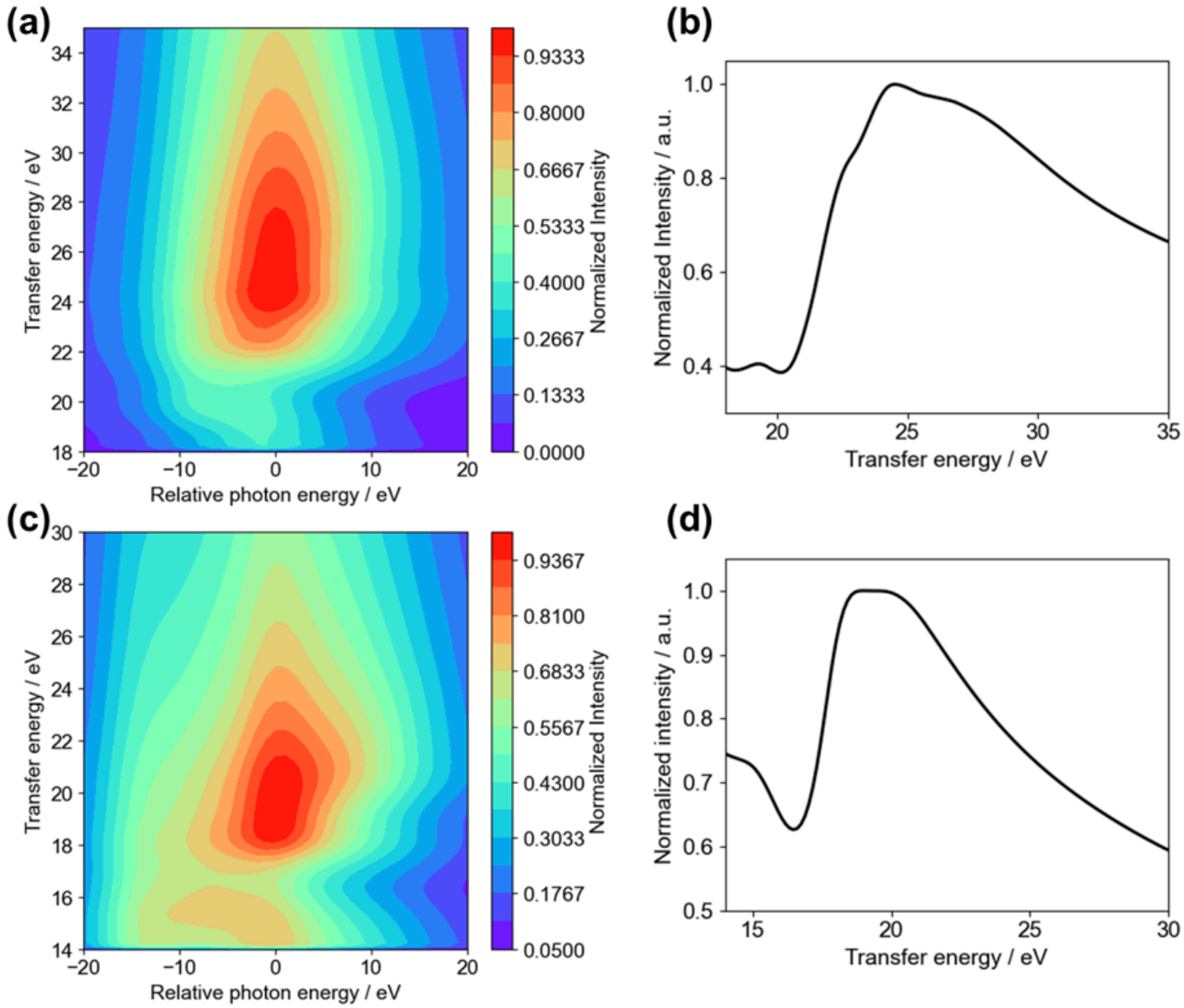


Figure 3

Simulated (a, c) Ln L_3-edge 2D RIXS maps and (b, d) corresponding transfer-energy profiles calculated using crystal-field-modified atomic multiplet models for (a, b) complex **1** (Tb) and (c, d) complex **2** (Dy).

Supplementary Files

This is a list of supplementary files associated with this preprint. Click to download.

- SI.docx
- 2.cif
- 1.cif